THE RESULTS OF AURORAL SOUNDING WITH S-310JA-4 ROCKET: ELECTRIC FIELD, PARTICLE AND WAVES

Hisao YAMAGISHI, Masaki EJIRI, Takeo HIRASAWA,
National Institute of Polar Research, 9-10, Kaga 1-chome, Itabashi-ku, Tokyo 173

Koichiro TSURUDA,
Institute of Space and Aeronautical Science, University of Tokyo, Komaba 4-chome, Meguro-ku, Tokyo 153

Iwane KIMURA
Department of Electrical Engineering, Kyoto University, Sakyo-ku, Kyoto 606

and

Masanori NISHINO
Research Institute of Atmospherics, Nagoya University, 13, Honohara 3-chome, Toyokawa 442

Abstract: The 310JA-4 rocket was launched perpendicular to the geomagnetic field line in the poleward direction from Syowa Station, Antarctica around the onset time of a small substorm (~ -140 nT). The rocket moved across aurora of the ray-band type. DC electric field, plasma waves in a frequency range from 20 Hz to 8 kHz, auroral energetic electron (>90 eV), electron density, and electron temperature were measured by onboard instruments.

The measured electric field directed generally northeastward, the fact being interpreted as a modification of a large scale electric field (directing northward (equatorward) in the morning sector of the auroral region) by an eastward polarization electric field in the precipitation region. Auroral energetic electron flux up to 8×10^8 electrons/cm^2·s and auroral hiss were observed during the flight, and they showed a close correlation.

1. Introduction

Auroral substorm injected particles cause strong disturbances in the polar ionosphere and generate various kinds of electrostatic and electromagnetic waves from ULF through ELF, VLF to HF bands, and such phenomena have been investigated by ground observation including remote sensing technique such as incoherent scatter radar and VLF doppler radar, and by *in situ* observation using satellites and rockets.

The characteristics of auroral particles such as energy spectra and pitch angle distribution have been investigated (ARNOLDY, 1974; HULTQVIST, 1974; BOYD, 1975; MILLER and WHALEN, 1976), and the physical processes in the ionosphere caused by

energetic particle precipitation have been investigated theoretically by many scientists (*e.g.* BANKS *et al.*, 1974; JONES and REES, 1973; ROBLE and REES, 1977).

Wave phenomena in the ionosphere during a substorm have been also investigated with many sounding rockets, from ELF range (KELLEY and MOZER, 1973; BERING *et al.*, 1975; OGAWA *et al.*, 1976; MORI *et al.*, 1979; OGAWA *et al.*, 1979) through VLF range (*e.g.* KIMURA *et al.*, 1980) to HF range (*e.g.* OYA *et al.*, 1980).

These phenomena are interconnected each other through plasma instabilities and wave-particle interactions. Therefore simultaneous observation of the related physical quantities is important to understand the mechanism of the phenomena. A comprehensively instrumented S-310JA-4 sounding rocket had been designed to carry out this objective and was launched from Syowa Station (geomagnetic latitude 70.0°, longitude 79.4°, $L=6.1$) at 003243 UT on August 18, 1978. The azimuthal direction of the rocket ground track was 129° from the geographic north (8.2° eastward from

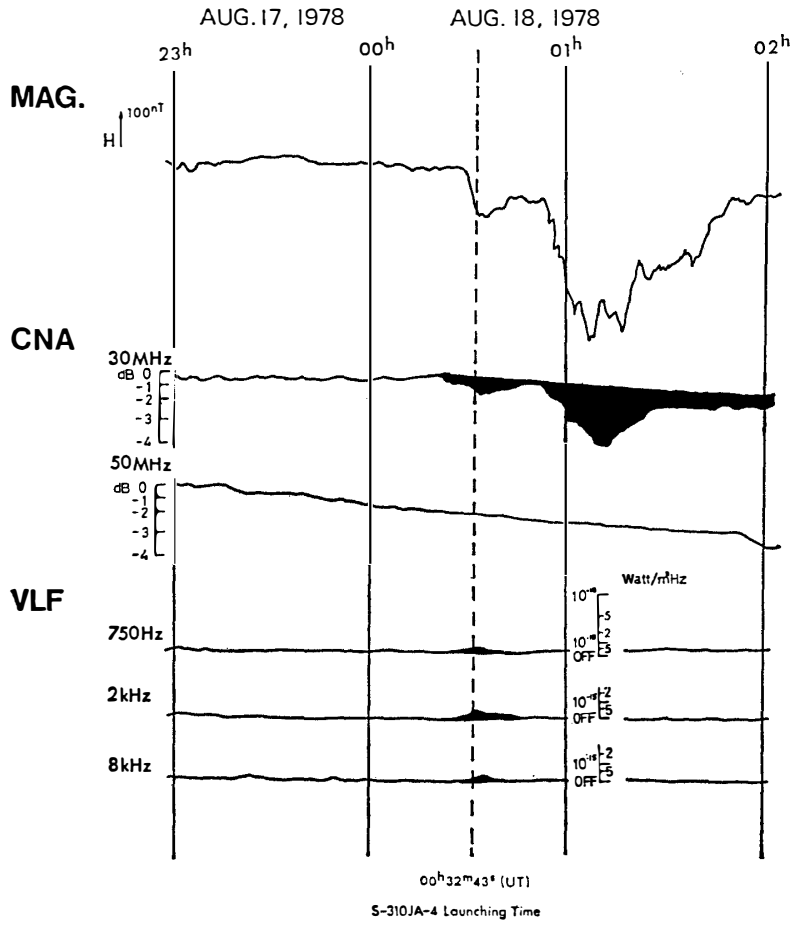

Fig. 1. Time variations of geomagnetic field, CNA and VLF noise intensities at 0.75, 2 and 8 kHz observed on the ground.

the geomagnetic south). A small auroral substorm started just before the launching. Fig. 1 shows the geomagnetic H component and 30 MHz cosmic noise absorption during the rocket flight, in which the launching time is indicated by a dashed line. This report describes the experimental results, and discusses the interrelation of observed physical quantities together with ground based geophysical observation data.

2. Experimental Results

2.1. Electron density profile

For electron density measurement, on the S-310JA-4 rocket installed were two types of instruments, a fixed biased spherical probe with its diameter of 3 cm and an RF impedance probe. Electron density measurements by the RF impedance probe were carried out every nine seconds, and the data were used to calibrate the electron density profile obtained by the fixed biased probe. Fig. 2 shows the current density profile of thermal electrons measured by the fixed biased probe. The potential of the probe was set at three volts above the potential of the rocket body. The probe current i is a function of electron density, electron temperature and probe potential as (MKS unit being used unless otherwise mentioned),

$$i=4\pi r^2 f_s(n_e e\sqrt{kT_e/2\pi m}) \tag{1}$$

and

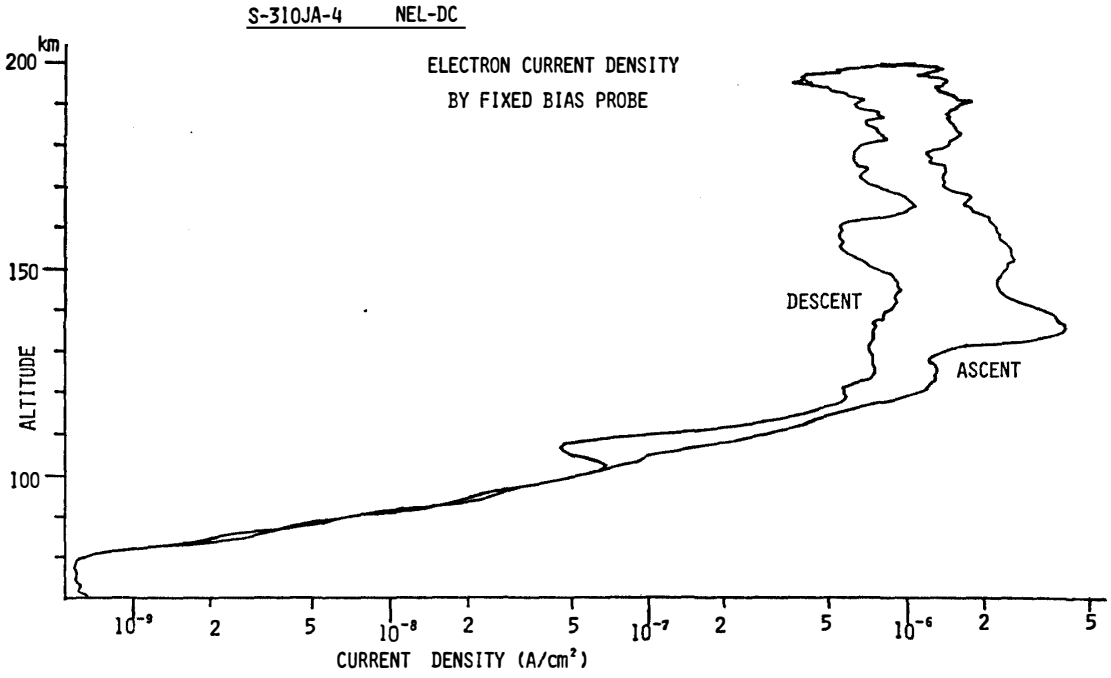

Fig. 2. Altitude variation of thermal electron current density measured by a fixed biased probe.

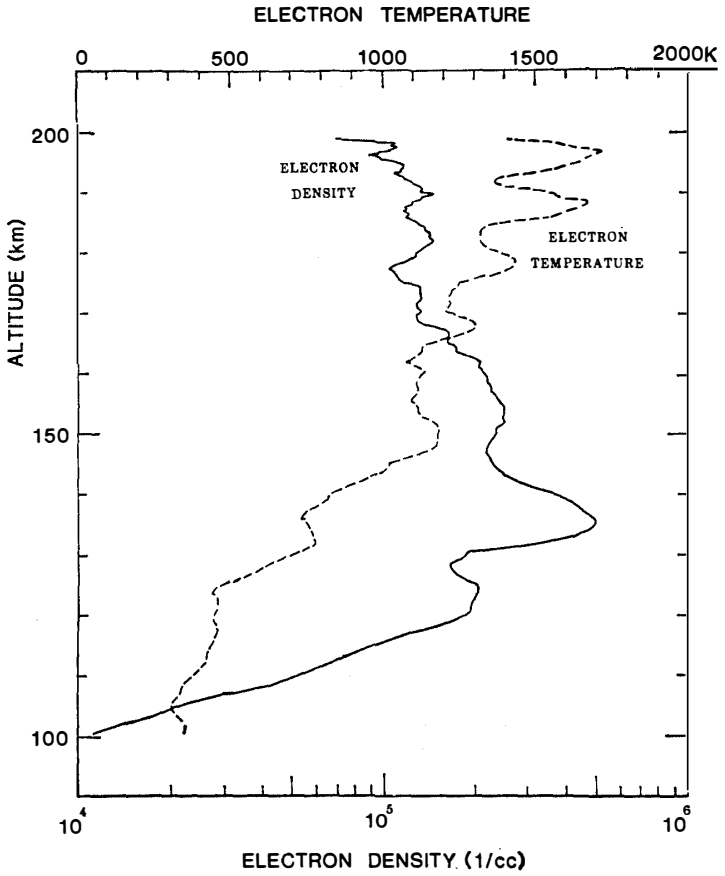

Fig. 3. Altitude variations of electron density (solid line) and electron temperature (dashed line).

$$f_s=(a/r)^2\left\{1-\frac{a-r}{a}\exp\left(\frac{r\eta}{a-r}\right)\right\} \tag{2}$$

where $\eta=eV/kT_e$, r radius of the probe, k Boltzmann constant, n_e electron density, e unit charge of electron, T_e electron temperature, m electron mass, a radius of ion sheath, and V probe potential with respect to the plasma potential, and f_s means the efficiency of collecting electrons in the ion sheath around the probe. In the present case, V and kT_e are assumed to be two volts and 0.1 volt respectively, as T_e is $\sim$1000 K. Then η becomes sufficiently large and f_s can be given as $(a/r)^2$. Equation (1) can, then, be expressed in a simplified form as,

$$i=4\pi a^2(n_e e\sqrt{kT_e/2\pi m}). \tag{3}$$

By using electron temperature data (K. OYAMA, private communication), electron density by RF impedance probe, and electron current by the fixed biased probe, "a" could be determined every nine seconds. By interporating this value, the electron

current i can be transformed to electron density. Fig. 3 shows the electron density profile during the ascent of the rocket flight, obtained by the procedures mentioned above. The electron temperature profile (K. OYAMA, private communication) is also shown in Fig. 3 by a dashed line. This electron density profile shows irregular enhancements with a scale size up to about 30 km. This enhancement could be caused by auroral particle precipitation confined in such a scale size of magnetic flux tube. The electron temperature profile also shows similar irregular variations, which are anti-correlated with the electron density variations. Especially in the altitude range above 170 km, both amplitudes of variations in electron density and temperature are 20%, so that the plasma pressure $n_e kT_e$ is thought to have been kept almost constant. The electron density profile shows its peak value at the altitude of 135 km. This altitude is considerably higher than those usually observed in more bright auroras in such cases as S-310JA-5, 6 and 7 rocket experiments which are reported in this issue. This fact suggests that the energy of auroral particles in this aurora could be rather low.

2.2. Particle observation by retarding potential analyzer

Auroral energetic electron flux was measured by a retarding potential analyzer with its aperture directed perpendicular to the rocket spin axis. The diameter of the aperture was 83 mm and a half angle of the aperture was 54°. As the retarding

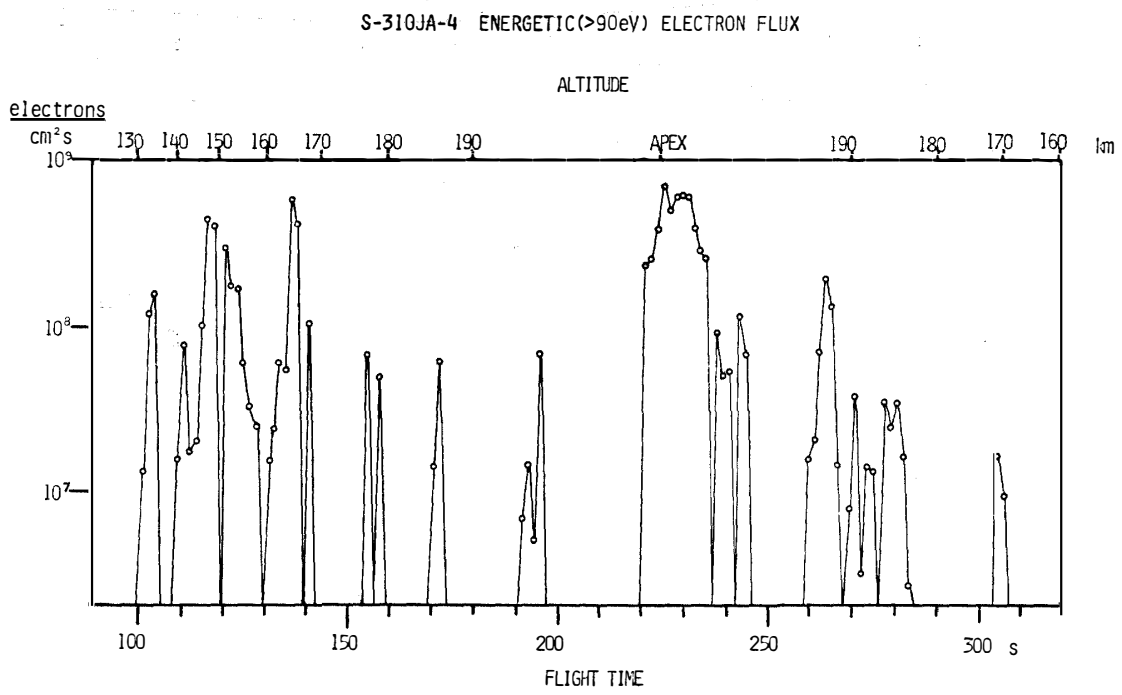

Fig. 4. Time variation of electron flux above 90 eV measured by the retarding potential analyzer.

potential was fixed at 90 V, electrons with their energies above 90 eV were measured by this instrument. The electron flux was observed intermittently during the flight as shown in Fig. 4. Maximum electron flux value up to 8×10^9 electrons/cm^2·s was observed near the apex.

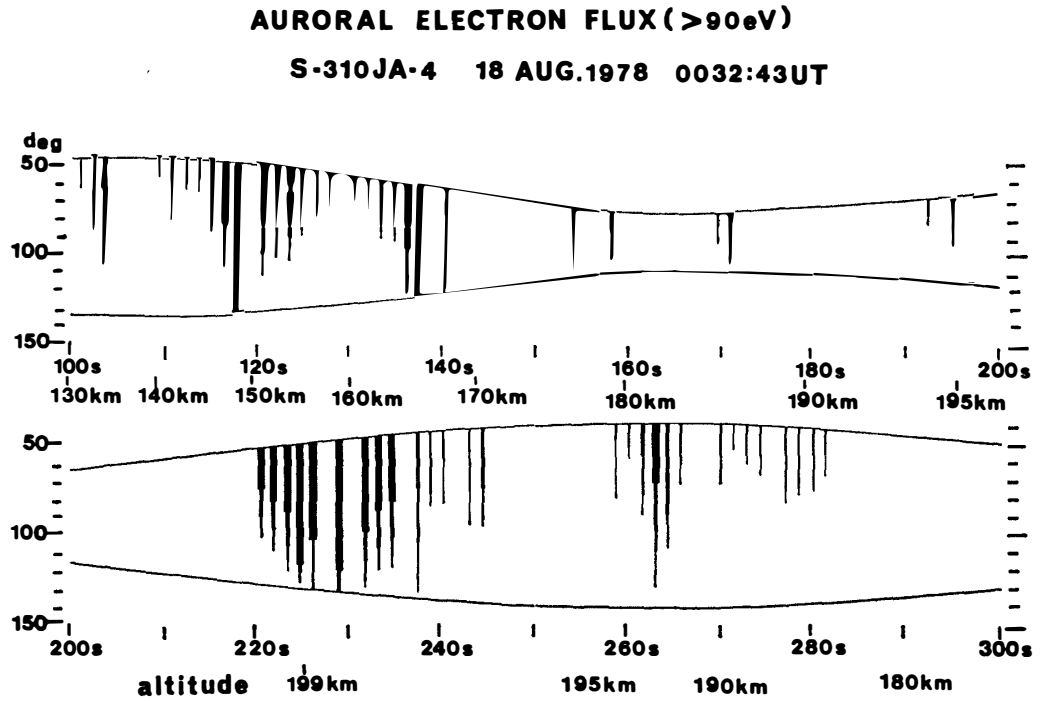

Fig. 5. Time variation of the sweep range of the aperature direction of the retarding potential analyzer and the relative quantity of electron flux.

The aperture angle was so wide that this analyzer did not have enough angle resolution, but a general tendency of pitch angle distribution could be obtained. In Fig. 5, the ordinate shows an angle between the direction of the aperture and the geomagnetic field line, and the solid curve shows a sweep range of the aperture direction during each spin period of the rocket. 0° indicates that the aperture is parallel to field line (upward) and 180° indicates that the aperture is antiparallel (downward). The amount of electron flux observed is shown by the width of a bar. From this figure it is clear that down going (precipitating) electron flux was predominant during the rocket flight.

From these figures, a time scale of the duration of particle precipitation was estimated to be from several seconds to several tens of seconds, and the horizontal extent of the precipitation area was up to ~30 km under the limitation of ambiguity between time and space caused by rocket motion. This time scale of precipitation was almost the same as the duration of auroral hiss emission observed by the VLF

receiver on board, which will be shown later. The spacial extent of the precipitation area was also comparable to the scale size of electron density enhancement shown in Fig. 3.

2.3. Electric field observation

DC electric field was measured by two pairs of double probes, consisted of two sets of insulated booms of 3.7 m and 7.65 m in length and four spherical probes attached at the tip of each boom. Each pair was separated by 60 cm along the rocket axis. In this analysis, data from the lower pair (7.65 m long) was used.

Fig. 6 shows the total DC electric field ($|\vec{E}+\vec{V}\times\vec{B}|$) observed by this double probe. The abscissa shows the field intensity and the ordinate shows the rocket altitude. $\vec{V}\times\vec{B}$ electric field induced by the rocket motion was also shown. In this rocket, two kinds of attitude sensor, a geomagnetic aspect sensor and an infrared horizon sensor were installed. From these data (F. TOHYAMA and M. ISHIDO, private communication) the rocket attitude was successfully determined as shown in Fig. 7,

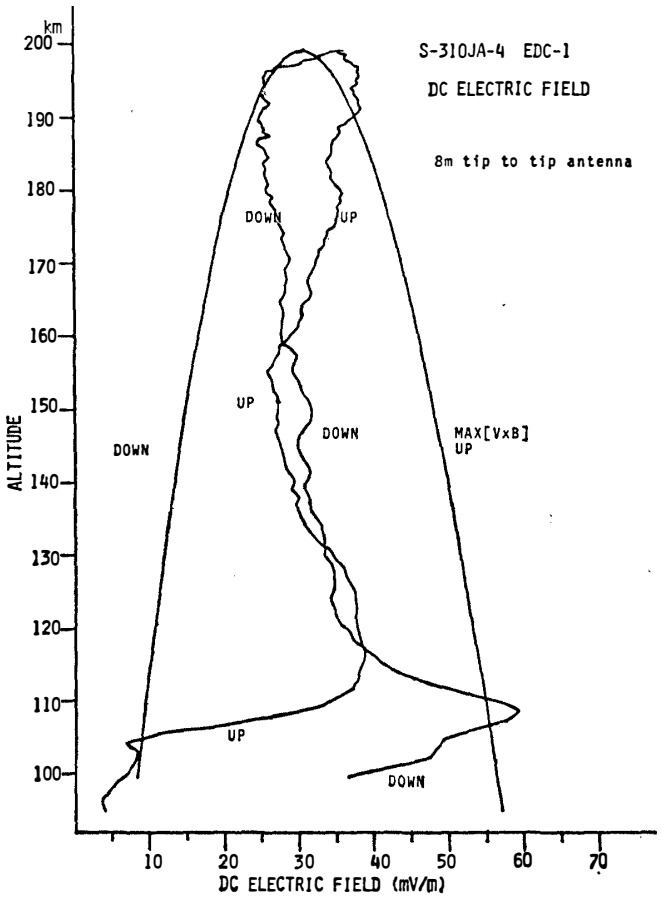

Fig. 6. Altitude variation of the observed DC electric field ($|\vec{E}+\vec{V}\times\vec{B}|$).

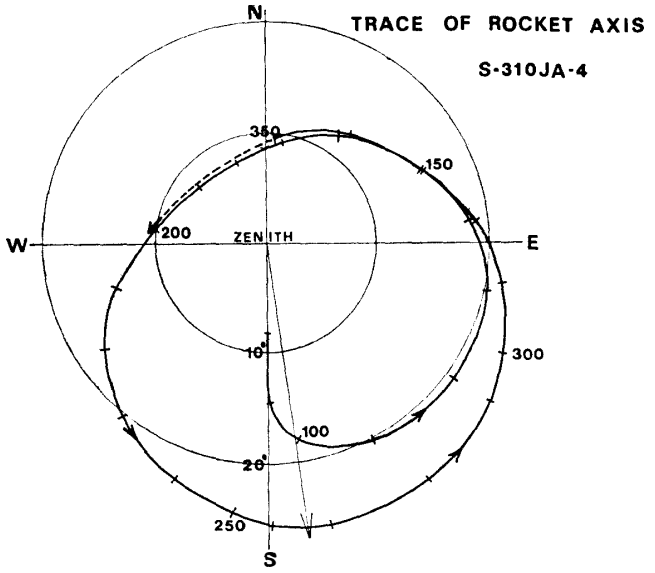

Fig. 7. Time variation of rocket axis direction plotted on a polar map.

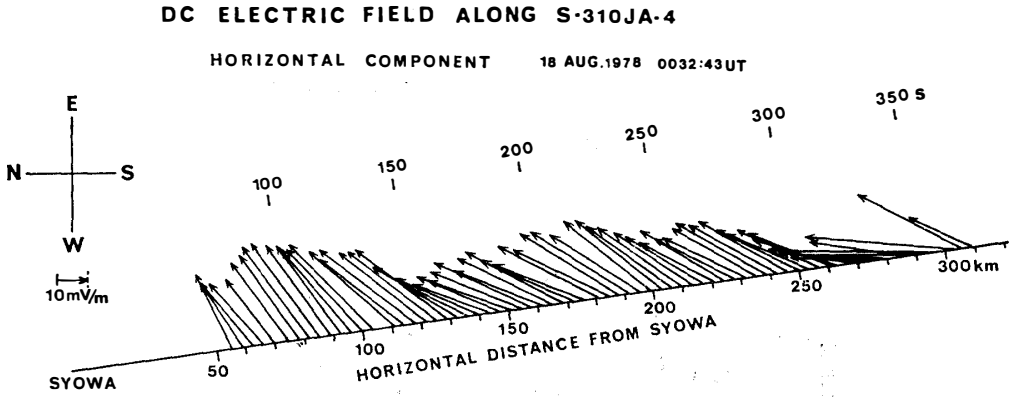

Fig. 8. Horizontal component of the DC electric field plotted along the rocket ground track.

where the rocket axis direction was plotted on a polar map. Using these data, apparent $\vec{V}\times\vec{B}$ electric field was subtracted from the observed electric field, then the electric field was transformed in the geomagnetic coordinate with an assumption that an electric field parallel to the geomagnetic field line is zero.

Fig. 8 shows the horizontal component of the electric field plotted along the rocket ground track in geomagnetic coordinate. The electric field pointed generally northeastward and the direction intermittently rotated northward.

Fig. 9 shows another expression of the horizontal electric field, where eastward and northward components were shown with the rocket flight time. The durations of auroral particle precipitation are indicated by bars. The eastward component

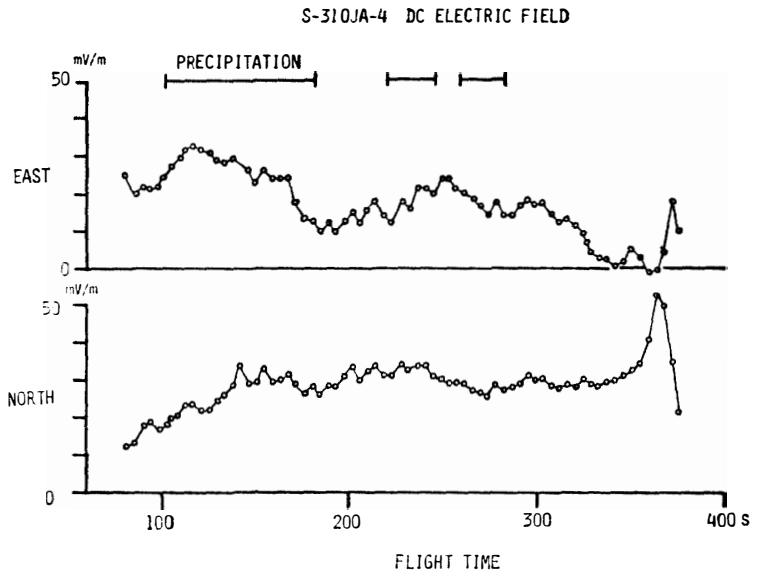

Fig. 9. Time variation of east and north components of DC electric field. Bar at the top indicates the duration of auroral particle precipitation.

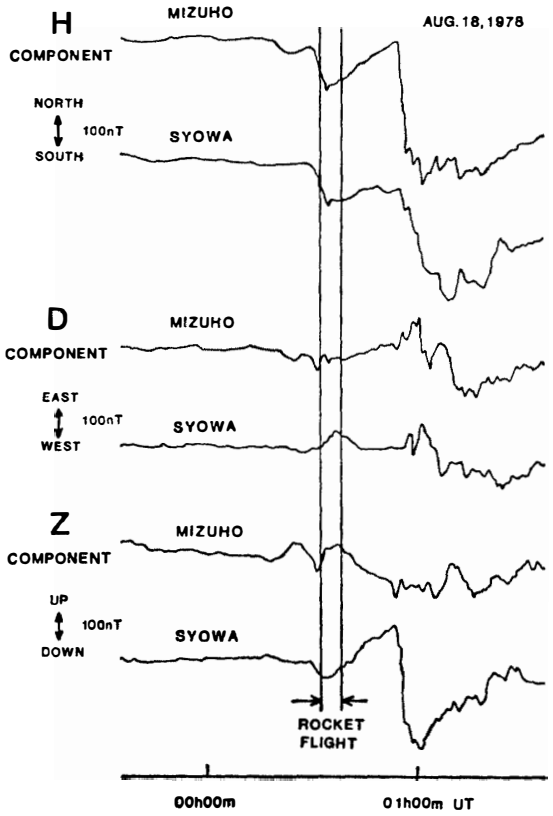

Fig. 10. Magnetogram of Syowa and Mizuho Stations at the time of the rocket flight.

seems to be enhanced during the precipitation period, the fact suggesting the effect of electric field induced by auroral particle precipitation.

Fig. 10 shows the magnetograms of Syowa Station and Mizuho Station, 250 km geomagnetically south of Syowa Station, at the time of the rocket flight. A decrease of H component (140 nT) at both stations and a decrease of Z component at Syowa Station indicate that the westward electrojet was streaming just poleward of Syowa Station, and the rocket seemed to have flown through the electrojet.

2.4. Observation of VLF wave emission

Waves in a VLF range from 20 Hz to 10 kHz were measured by three orthogonally crossed loop antennas and four spherical probes at the tips of insulated booms, which were also used as a double probe for an electric field measurement. A fixed biased probe used for electron density measurement was also used for plasma waves measurement in a frequency range from 20 Hz to 10 kHz.

Observed data in lower frequency range from 20 Hz to 200 Hz were transmitted by IRIG FM telemetry channel, and the data in upper frequency range from 200 Hz to 10 kHz were transmitted by a VSB wide band telemetry channel.

Figs. 11 and 12 show frequency-time (f-t) diagrams of wave electric field in the upper and lower frequency ranges. The numbers under each pannel indicate flight time after launch in seconds and altitude of the rocket. The sensors were deployed at 59 seconds, therefore the data before 59 seconds have no physical meaning. In Fig. 11 enhanced broad signals are seen in the altitude range between 100 km and 140 km during the ascent. These might be electrostatic waves often observed by sounding rockets in this altitude range in the polar ionosphere (OGAWA *et al.*, 1979).

Another type of broad band emissions was observed from 197 seconds to 235 seconds. This shows strong spin modulation and sharp lower cutoff near 4.5 kHz. Bars drawn above each pannel in Fig. 11 indicate the duration of auroral particle precipitation. Strong particle precipitation started at 220 seconds, and an enhancement of this emission coincides with this precipitation very well. From these features, this emission was considered to be auroral hiss emission generated by auroral particle.

Another wide band channel was used, by time sharing, for the wave magnetic field and the electron density fluctuation data. Fig. 13 shows an f-t diagram of this wide band channel. The first half of the diagram before 225 seconds shows the wave magnetic field observed by a loop antenna and the second half after 226 seconds shows the electron density fluctuation observed by a fixed biased probe. As for the wave magnetic field data, constant frequency components near 3.5 kHz, 6 kHz, 7.5 kHz and 9.5 kHz, and a fluctuating frequency component near 2 kHz are caused by an interference with other telemetry channels. Except for these, no predominant signal can be seen.

Comparing with Fig. 11, auroral hiss emission between 195 seconds and 270 seconds has no counterpart in the f-t diagram of the wave magnetic field in Fig. 13.

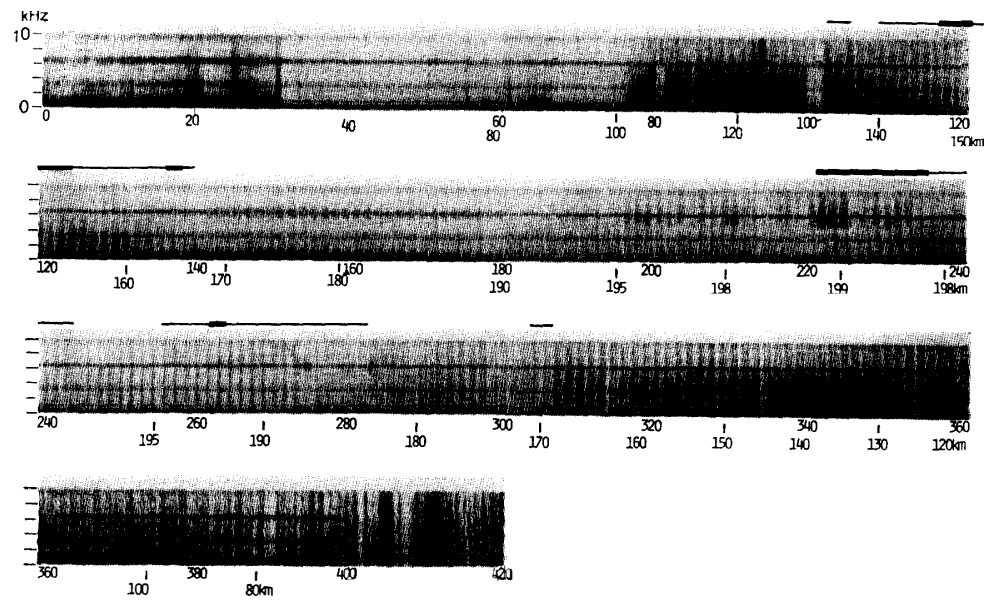

Fig. 11. F-t diagram of wave electric field in VLF range.

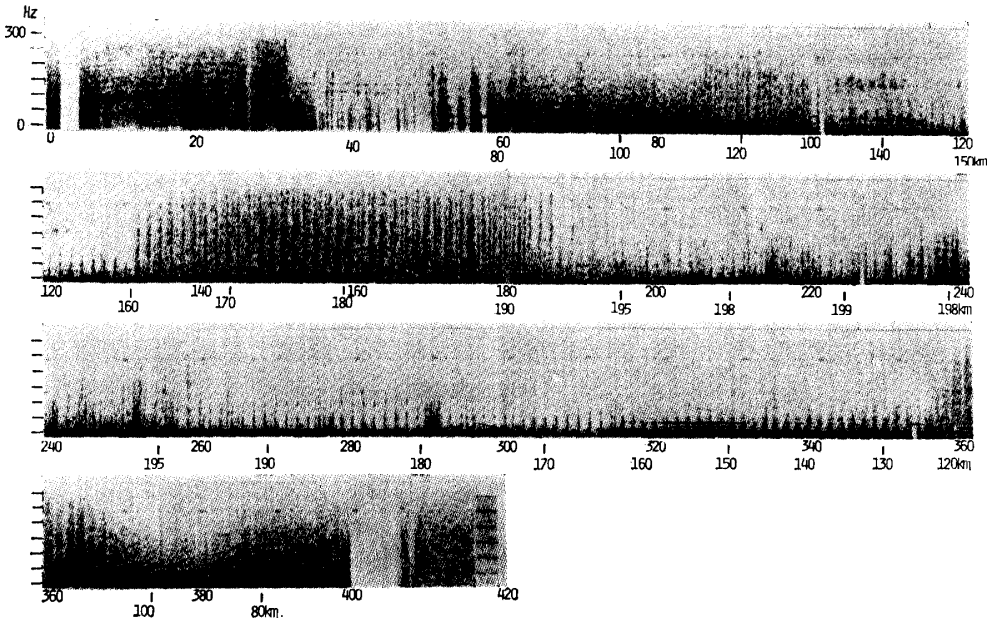

Fig. 12. F-t diagram of the wave electric field in ELF range.

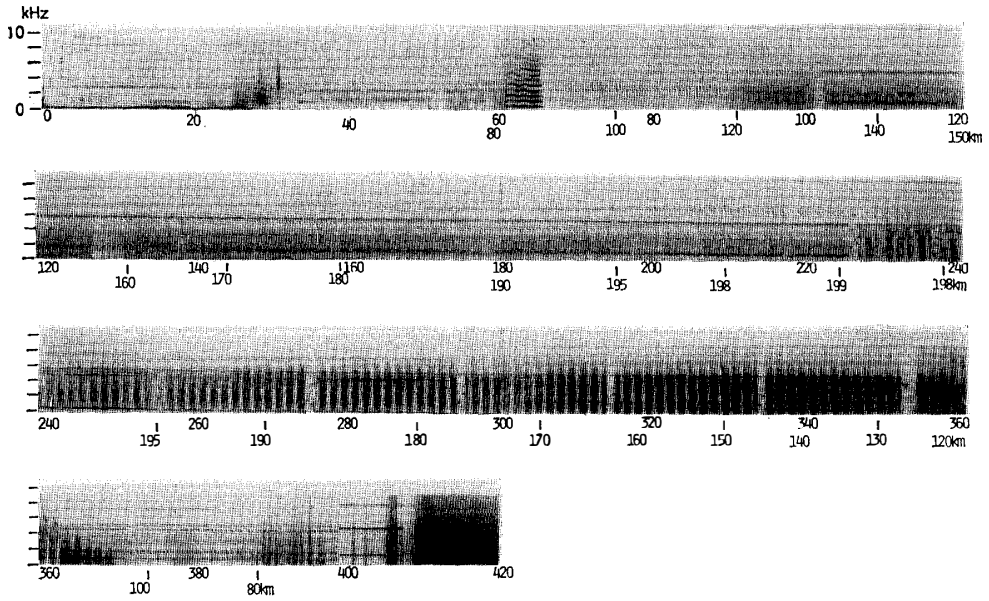

Fig. 13. F-t diagram of the wave magnetic field (the first half) and the electron density fluctuation (the second half) in VLF range.

The absolute value of the wave magnetic field in a frequency range from 5 kHz to 9 kHz at this time is calculated to be 0.2 $m\gamma/\sqrt{Hz}$, which is almost the same as the receiver noise level. Comparing this magnetic field intensity with observed wave electric field of 1.5 $\mu V/m\sqrt{Hz}$, the refractive index is calculated to be 40, assuming the whistler mode propagation along the geomagnetic field line.

The magnetic field spectrum in the above frequency range is stable in time, and does not show lower cutoff characteristics observed in the wave electric field spectrum. Therefore there is a possibility that the wave magnetic field is smaller than 0.2 $m\gamma/\sqrt{Hz}$, and masked by receiver noise level. In this case, observed auroral hiss shows rather electrostatic characteristics.

3. Discussions

S-310JA-4 measured an electron density profile in a ray-band type aurora. It shows an irregular variation in electron density, and is a little bit different from those observed by S-310JA-5, -6 and -7. In Fig. 14, for example, electron density profiles obtained by S-310JA-4 and -5 during the ascent are illustrated. A possible reason for such difference is that S-310JA-4 was launched southward and moved across the geomagnetic flux tubes during the ascent. On the other hand, the other rockets were

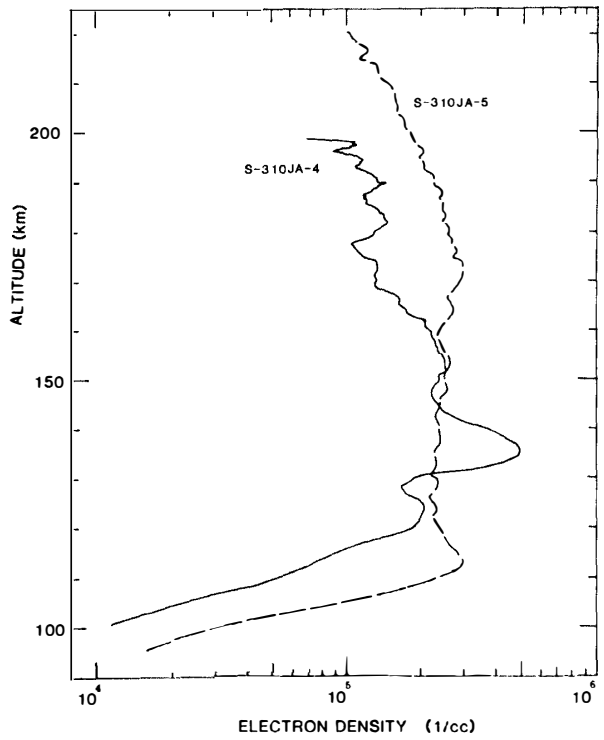

Fig. 14. Comparison of electron density profiles observed by S-310JA-4 (solid line) and S-310JA-5 (dashed line) during ascent of rocket flight.

flown northward and moved along the geomagnetic field lines, along which the electron density changes smoothly according to the diffusive equilibrium condition. Another possible reason is that such a difference could be attributed to the different spatial distribution for particle precipitation, namely the difference between ray-band type aurora and corona type or bright arc aurora.

Such a horizontal electron density inhomogeneity is possible in the auroral ionosphere, and this fact indicates that the diffusion across the geomagnetic field lines is not efficient, and once the electron density was enhanced in some magnetic flux tube, the enhancement lasted for a pretty long time. JONES and REES (1973) studied time dependent response of the ionospheric electron density against the auroral particle precipitation. They got the results that the build up time of electron density was several seconds at 100 km and a few minutes at 200 km altitude after the beginning of precipitation. As for the decay time after the cessation of precipitation, they showed one minute at 100 km and nearly ten minutes at 200 km altitude.

Fig. 15 shows the correlation between auroral electron precipitation and electron density enhancement, where the precipitation area is shown by hatching. Poor correlation between them is considered to be due to the slow response of the ionosphere

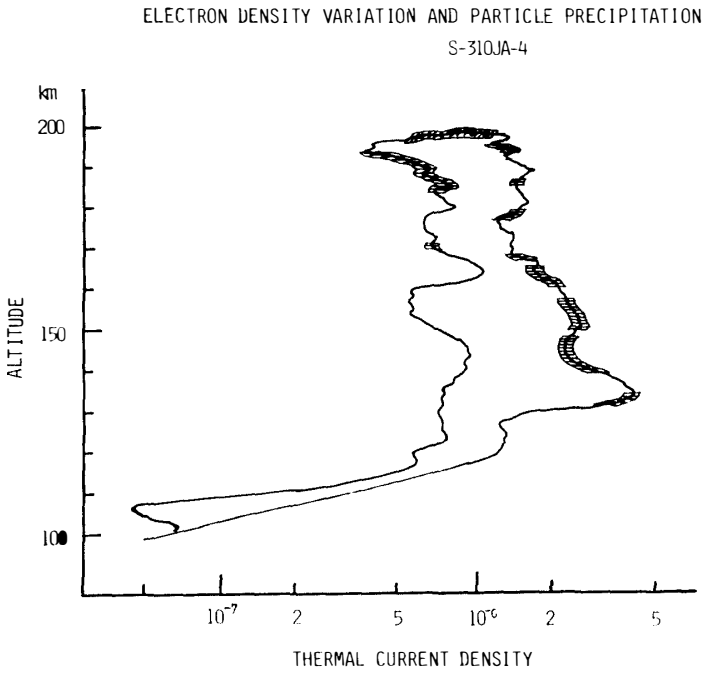

Fig. 15. Comparison of electron density enhancement and the area of auroral particle precipitation (shown by hatching).

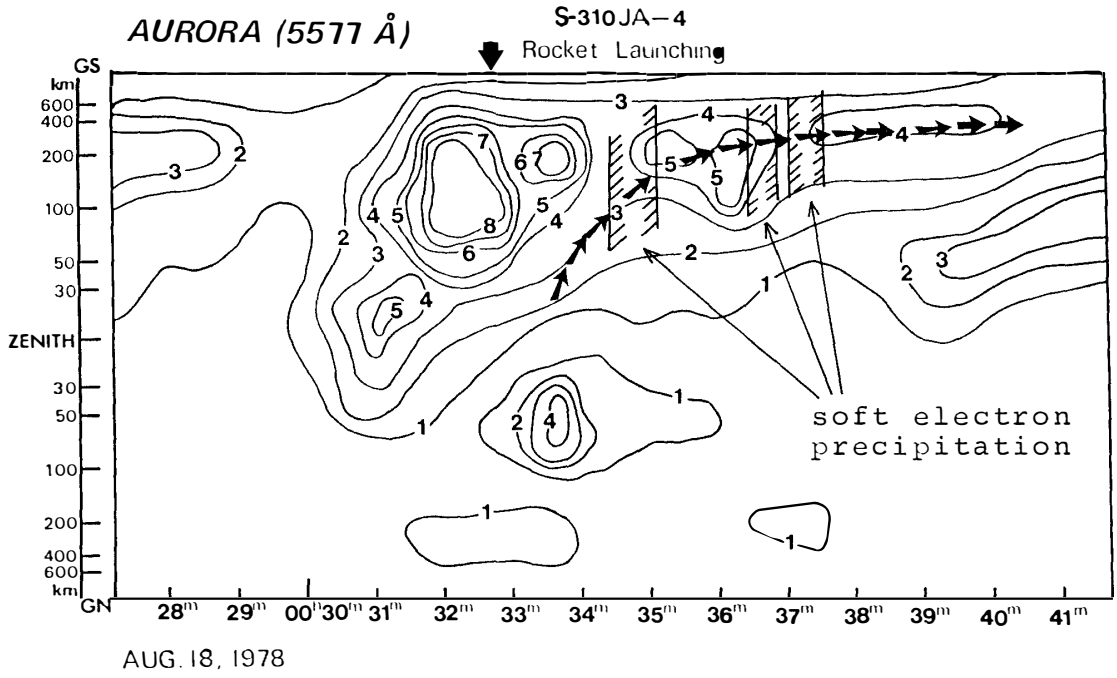

Fig. 16. Equicontour lines of 5577 Å auroral photo emission intensity with time. The rocket trajectory is shown by solid arrows. The number associated with each contour denotes the 5577 Å intensity in kR.

mentioned above, and the observed electron density irregularity could be the after-effect of particle precipitation.

Next, let us consider the relation between the auroral electron precipitation and the auroral luminosity. Equicontours of 5577 Å meridian scanning photometer data observed at Syowa Station are shown in Fig. 16, in which the rocket trajectory projected down to 100 km altitude along the geomagnetic field lines is indicated by arrows. The number on each contour line indicates intensity of auroral photo emission in kilo Rayleigh. The aurora showed southward (poleward) drift with decreasing intensity, and the rocket also moved southwards following the auroral motion. The area of precipitation is shown by hatching in this figure. The electron flux increases where the luminosity is low and decreases where the luminosity is high.

Energy spectra of auroral electrons near the auroral arc have been investigated by rockets and satellites (*e.g.* ARNOLDY and CHOY, 1973; MENG, 1976; MENG *et al.*, 1978), obtaining the results that the energy spectra have a peak near 3 keV in bright aurora, 0.5–1.2 keV in faint aurora, and near 8 keV in westward traveling surge. Rocket observations of auroral electrons (CHOY and ARNOLDY, 1971; BERING *et al.*, 1975) also report the finding that the soft electron flux from a few tens of eV to several hundred eV increases at the edge or just poleward of auroral arc by nearly one order of magnitude greater than in the arc with its spatial width of a few tens of km. The magnitude of this flux is much greater than those responsible for the luminosity.

In our experiment, a retarding potential analyzer was used for particle observation. This instrument was designed to measure soft electron flux with its energy above 90 eV, and does not have enough sensitivity to harder electrons which are responsible for auroral luminosity. Therefore, the observed electron flux is thought to be those soft electrons mentioned above, and this is the reason why the observed precipitation area does not coincide with auroral luminosity.

Comparing Fig. 9 with Fig. 10, let us consider the consistency between the electric field observed by the rocket and the ionospheric current expected from the magnetogram of the ground stations, Syowa and Mizuho Stations. Decrease in H component at both stations and decrease in Z component at Syowa Station indicate that a westward electrojet was streaming on the poleward side of Syowa Station. During the substorm, ionospheric Hall conductivity σ_H is much larger than Pedersen conductivity σ_P, (*e.g.* HORWITZ *et al.*, 1978), so this jet current is thought to be driven by northward electric field component E_N. Therefore the variation of geomagnetic field H component (ΔH) is consistent with E_N. The eastward component E_E drives northward Hall current and this indicates westward magnetic field on the ground. But the observed D component shows opposite variation.

BREKKE *et al.* (1974) studied the correlation between ionospheric currents observed by an incoherent scatter radar and geomagnetic field variations on the ground. They obtained similar results, that the variation of east-west current agrees better with ΔH than does north-south current with ΔD.

Ionospheric electric field is considered to be the projection of large scale electric field in the magnetosphere under the assumption of equipotential geomagnetic field line. The rocket was launched at 003243 UT, which is almost the same as the MLT of Syowa Station, therefore the rocket is supposed to have observed northward (equatorward) electric field just dawnside of Harang discontinuity. However the rocket observed N to NE electric field, so possible mechanism producing eastward electric field component should be considered.

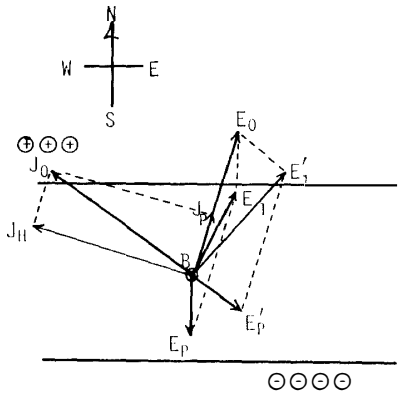

Fig. 17. Configuration of ionospheric electric field and induced current arround the conductive belt in the dynamo region. E_o, E_p, E_1 denotes primary electric field, polarization electric field and resultant electric field respectively. J_H, J_P, J_T denotes Hall current, Pedersen current and the total current, respectively.

From the magnetogram of Syowa and Mizuho Stations (Fig. 10), westward electrojet was supposed to stream on the poleward side of Syowa Station, therefore, a belt of electric conductivity enhancement was expected to extend in the east-west direction. Fig. 17 illustrates a possible relation between the electric field and induced current in the ionosphere. Primary electric field E_0 is assumed to direct NNE, (almost equatorward) which is the projection of large scale magnetospheric electric field in the morning sector near Harang discontinuity, and the high conductivity belt is assumed to extend in the east-west direction. E_o induces Hall current J_H and Pedersen current J_p, and total current J_T causes charge accumulation at the both sides of the conductive belt, then this charge induces a polarization electric field E_p. If the conductive belt has finite length in the east-west direction, the polarization field has eastward component, shown as E_p'. In both cases, electric field tends to rotate eastward and Hall current reduces. If the field aligned current is allowed to flow along the edge of this conductive belt, northward current component can be closed with the field aligned current, and no charge separation occurs. In such case, primary electric field can be maintained. NNE electric field observed from 170 seconds to 210 seconds and northward electric field observed after 320 seconds can be explained as the latter case, and the rest can be explained as the former case. More qualitative analysis is required for drawing a correct picture to explain this observed electric field.

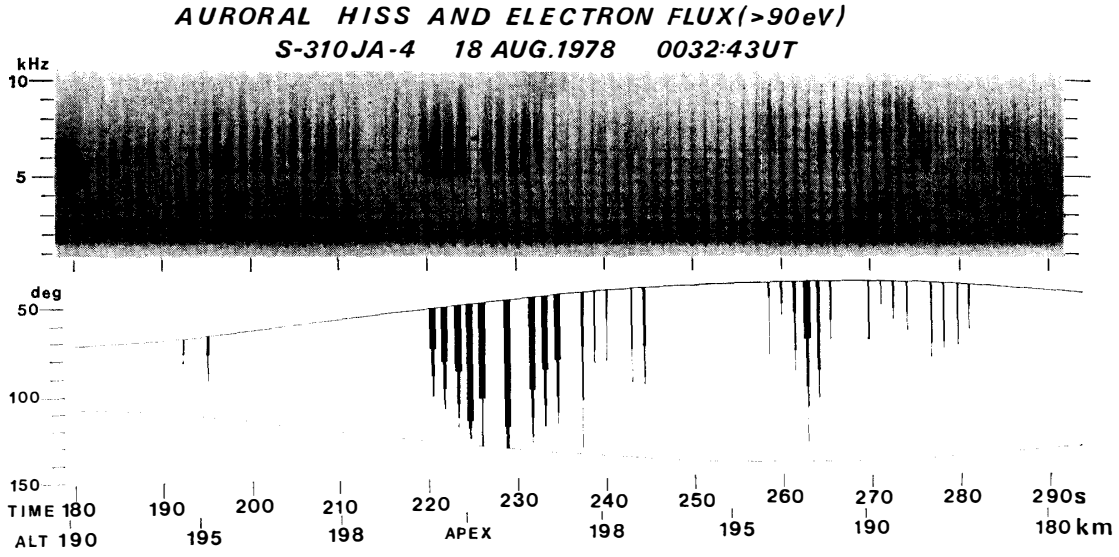

Fig. 18. Correlation between auroral hiss emission (top pannel) and auroral particle precipitation (bottom pannel).

Fig. 18 shows the correlation between the auroral hiss and the auroral particle observed by this rocket. Auroral particle precipitates along geomagnetic field line, and is thought to be confined in latitudinally narrow (a few tens of kilometer) area. However auroral hiss generated by such particle can propagate widely and is expected to be observed in much wider area. Before 210 seconds, auroral hiss was observed but the rocket could not observe auroral particle. This may be such the case mentioned above that the rocket flew outside of precipitation region and only the wave emission could be observed.

Attention should be paid to the coincidence of particle precipitation and hiss emission after 220 seconds. Auroral hiss has been considered to be generated by Cerenkov radiation from auroral particles at the altitude of several thousand kilometers. If we assume the source region of auroral hiss at such altitude, ray path study of auroral hiss by MAKITA (1978) shows that the ray path tends to move away from the geomagnetic field line to low latitude side. Considering the narrow width of precipitation area, such coincidence between hiss emission and particle precipitation suggests that the source region of this auroral hiss was not much far from the observed area.

4. Conclusion

The S-310JA-4 rocket was launched into a ray band type aurora, and ionospheric electric field, electron density profile, auroral particle and waves were successfully observed during its flight.

The following is the summary of the observed facts.

(1) Irregular electron density variation with its scale size of a few tens of kilometers is observed. This variation is anticorrelated with the observed electron temperature. This fact indicates that plasma pressure $n_e k T_e$ is thought to have been kept almost constant along the geomagnetic flux tube.

(2) Auroral energetic electron flux with its energy above 90 eV was observed intermeittently during the flight. This flux comes downwards and the maximum flux is 8×10^8 electrons/cm^2·s. This flux is observed where the auroral luminosity is low.

(3) DC electric field directs geomagnetically NE while the auroral electron flux is observed, and it directs NNE when the electron flux decreases. The northward electric field component is consistent with the decrease of geomagnetic H component observed on the ground, but the eastward electric field component does not agree well with the variation of geomagnetic D component.

(4) Band limited auroral hiss emission with its electric field intensity 1.5 μV/m$\sqrt{\text{Hz}}$ is observed. This shows a close correlation with auroral particle precipitation.

The fact No. 1 indicates that spatially confined auroral particle precipitations mentioned as the fact No. 2 causes local electron density enhancement of a few tens of percents along geomagnetic field line which lasts for a pretty long time. This time scale is thought to be nearly ten minutes at 200 km altitude (JONES and REES, 1973).

The discrepancy between the auroral luminosity and particle precipitation mentioned as the fact No. 2 can be attributed to the difference of energy range between the observed electron flux (a few hundred eV) and those responsible for luminosity (one to a few keV).

Close correlation between auroral hiss and particle precipitation mentioned as the fact No. 4 indicates that the wave is thought to be generated not far from the rocket altitude, possibly several hundred kilometers, considering the ray path of the auroral hiss from the source region to the ionosphere.

Acknowledgments

We wish to express our thanks to the members of the 19th wintering party of Japanese Antarctic Research Expedition for their effort for rocket launching and data acquisition of ground based geophysical observations.

We are also grateful to the following staff for providing us with data observed by S-310JA-4 and -5 rockets; Prof. M. TOYODA and Dr. M. ISHIDO of Kobe University and to Prof. I. AOYAMA and Dr. F. TOHYAMA of Tokai University for rocket aspect data, to Dr. K. OYAMA of Institute of Space and Astronautical Science for electron temperature data, to Prof. H. OYA and Mr. T. TAKAHASHI of Tohoku University for electron density data.

Finally we are grateful to Dr. R. FUJII for valuable discussions on interpreting electric field data.

References

ARNOLDY, R. L. (1974): Auroral particle precipitation and Birkeland currents. Rev. Geophys. Space Phys., **12**, 217–231.

ARNOLDY, R. L. and CHOY, L. W. (1973): Auroral electrons of energy less than 1 keV observed at rocket altitude. J. Geophys. Res., **78**, 2187–2200.

BANKS, P. M., CHAPPEL, C. R. and NAGY, A. F. (1974): A new model for the interaction of auroral electrons with the atmosphere: Spectral degradation, backscatter, optical emissions, and ionization. J. Geophys. Res., **79**, 1459–1470.

BERING, E. A., KELLEY, M. C. and MOZER, F. S. (1975): Observations of an intense field aligned thermal ion flow and associated intense narrow band electric field oscillations. J. Geophys. Res., **80**, 4612–4620.

BOYD, J. S. (1975): Rocket-borne measurements of auroral electrons. Rev. Geophys. Space Phys., **13**, 735–740.

BREKKE, A., DOUPNIK, J. R. and BANKS, P. M. (1974): Incoherent scatter measurement of *E* region conductivities and currents in the auroral zone. J. Geophys. Res., **79**, 3773–3790.

CHOY, L. W. and ARNOLDY, R. L. (1971): Field-aligned particle currents near auroral arc. J. Geophys. Res., **76**, 8279–8298.

HORWITZ, J. L., DOUPNIK, J. R. and BANKS, P. M. (1978): Chatanika radar observations of the latitudinal distributions of auroral zone electric fields, conductivities, and currents. J. Geophys. Res., **83**, 1463–1481.

HULTQVIST, B. (1974): Rocket and satellite observations of energetic particle precipitation in relation to optical aurora. Ann. Geophys., **30**, 223–257.

JONES, R. A. and REES, M. H. (1973): Time dependent studies of the aurora I. Ion density and composition. Planet. Space Sci., **21**, 537–557.

KELLEY, M. C. and MOZER, F. S. (1973): Electric field and plasma density oscillations due to the high-frequency Hall current two-stream instability in the auroral *E* region. J. Geophys. Res., **78**, 2214–2221.

KIMURA, I., MATSUO, T., KAMADA, T. and NAGANO, I. (1980): Auroral hiss observed by Antarctic rockets, S-210JA-20 and 21. Nankyoku Shiryô (Antarct. Rec.), **69**, 17–36.

MAKITA, K. (1978): VLF-LF hiss emissions associated with aurora. Mem. Natl Inst. Polar Res., Ser. A (Aeronomy), **16**, 95–104.

MENG, C. -I. (1976): Simultaneous observation of low energy electron precipitation and optical auroral arcs in the evening sector by DMSP 32 satellite. J. Geophys. Res., **81**, 2771–2785.

MENG, C. -I., SNYDER, A. L., JR. and KROEHL, H. W. (1978): Observation of auroral westward traveling surges and electron precipitations. J. Geophys. Res., **83**, 575–584.

MILLER, J. R. and WHALEN, B. A. (1976): Characteristics of auroral proton precipitation observed from sounding rockets. J. Geophys. Res., **81**, 147–154.

MORI, H., OGAWA, T. and MIYAZAKI, S. (1979): Roketto ni yoru kyokuiki denrisô purazuma no jôran no kansoku (Rocket observations of plasma irregularities in the auroral ionosphere). Nankyoku Shiryô (Antarct. Rec.), **65**, 36–44.

OGAWA, T., MORI, H. and MIYAZAKI, S. (1976): Rocket observations of electron density irregularities in the antarctic auroral *E* region. J. Geophys. Res., **81**, 4013–4015.

OGAWA, T., MORITA, M., FUKUNISHI, H., MATSUO, T. and YOSHINO, T. (1979): Nankyoku roketto S-210JA-24, 25-gôki ni yoru denrisô denba no kansoku (Measurements of ionospheric

electric fields with Antarctic sounding rockets S-210JA-24 and 25). Nankyoku Shiryô (Antarct. Rec.), **63**, 252–275.

OYA, H., MIYAOKA, H. and MIYATAKE, S. (1980): Nankyoku roketto S-210JA-21-gôki ni yoru kô-shûha purazuma hadô supekutoru no kansoku (Observation of HF plasma wave spectrum at ionospheric level using sounding rocket S-210JA-21 in Antarctica). Nankyoku Shiryô (Antarct. Rec.), **69**, 37–51.

ROBLE, R. G. and REES, M. H. (1977): Time dependent studies of the aurora: Effects of particle precipitation on the dynamic morphology of ionospheric and atmospheric properties. Planet. Space Sci., **25**, 991–1010.

(Received September 1, 1980; Revised manuscript received December 22, 1980)